Manifolds optimization for the ATLAS Transition Radiation Tracker CO_2 cooling system

Joël Grognuz

Conseil Européen pour la Recherche Nucléaire, CH-1211 Genève 23

January 16, 2004

Abstract

Inlet and outlet manifolds represent a crucial part of the CO_2 cooling system for the ATLAS Transition Radiation Tracker (TRT) as long as they determine the flow homogeneity in the detector and the pressure losses where the hydraulic diameters are the smallest. An experiment was done on real scale prototypes with air. It is shown how the nozzle flow resistance coefficient variation along the inlet manifold simplifies its optimization compared to the outlet manifold. A flow model was developed to be able to optimize the system for turbulent flows from 25 $m^3\,h^{-1}$ to 75 $m^3\,h^{-1}$ and adapt the results to CO_2. For 50 $m^3\,h^{-1}$, a flow variation lower than 24% for both manifolds with an overall pressure drop of 92 mbar was obtained.

1 Requirements

The major problem in the design of the cooling system for the Transition Radiation Tracker (TRT) comes from the large CO_2 flows required (Q_{tot} = 50 $m^3\,h^{-1}$, 25 $m^3\,h^{-1}$ and 75 $m^3\,h^{-1}$ respectively for group of wheels of type A,B and C [1]) and a pressure regulation requirement within $\pm\,3$ mbars relative to the pressure around the detector wheels [2] to avoid damaging the detector. In terms of costs and risks, this regulation is facilitated by a minimization of the pressure drop on the whole system hence the requirement of a low pressure drop on the manifolds. The variation of the flux along the manifolds has also to be minimized to avoid having to increase the total flux in the system to cool efficiently the less ventilated parts, which would in turn increase the overall pressure drop or create undesirable temperature gradients in the detector.

2 Experiment

For symmetry reasons, two linear mock-ups of only a half of the inlet and outlet manifolds were built with a 1.5 mm thick plexiglas rectangle glued on an aluminium U shaped rail. For the inlet manifold, 40 holes were drilled in the plexiglas with 50 mm spacing at 3.5 mm from the edge. The inside cross section was rectangular with 42 x 7 mm edges. The cross section of the outlet manifold was 52 x 6.35 mm and the holes spacing 63.9 mm for 48 holes. The coordinate frame is chosen such that the z-axis lies along the manifold and points towards its closed end.

Additional holes drilled in the plexiglas allowed static pressure measurements along the manifold with a water U shaped manometer.

The flow through the nozzles, q_{nozzle}, was measured with the glass of a Vögtlin V100 ball flow-meter put directly on the nozzles. The nozzle flow measurements were only accurate for pressures larger than 12 mbar, below which the pressure loss through the flow-meter influenced the flow distribution along the manifold. For all measurements, it was checked that the total flow summed from the nozzle measurements was equal to the total flow Q_{in} or Q_{out}, respectively for the flow through the inlet and outlet manifold mock-ups, which was measured with a Wisag 2000 series flow-meter.

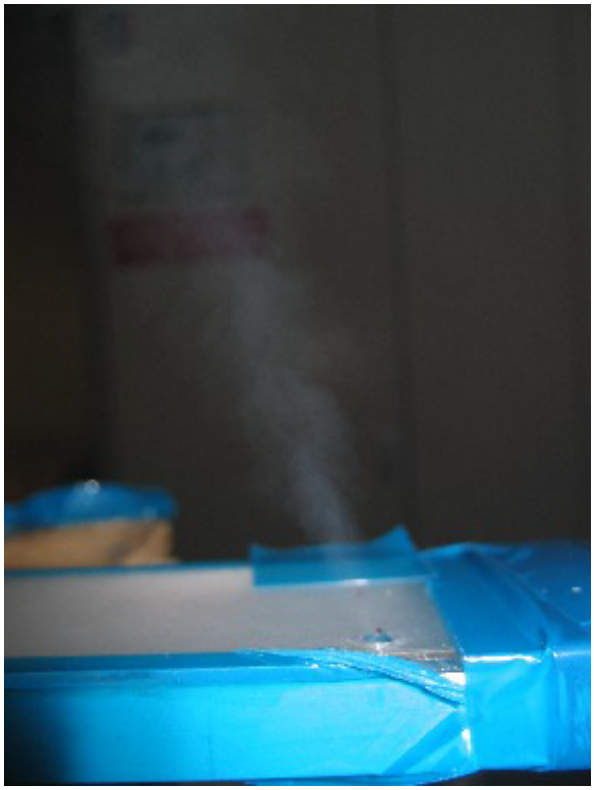

Figure 1: Flow out of the first nozzle of the inlet manifold, for which $\frac{Q_\perp}{q_{nozzle}}$ is the highest. The flow out of the upstream half of the hole is null; $c_{area} \approx 0.5$.

3 Model

The gas is assumed incompressible (M< 0.3) and the optimization model developed by Per Skarby [3] was adapted.

3.1 Flow through the nozzles

The flow through one nozzle is characterized by the fluid resistance coefficient;

$$\zeta = \frac{\Delta p_{nozzle}}{\frac{1}{2}\rho v^2} \qquad (1)$$

Where Δp is the pressure drop through the nozzle and $\frac{1}{2}\rho v^2$ the dynamic pressure. ζ depends on the geometry of the flow at the nozzle. It was indeed discovered that an effective area coefficient c_{area} for the nozzle aperture can be introduced in the following way:

$$\zeta = \frac{\zeta_0}{c_{area}^2} = \frac{\Delta p_{nozzle}\, a^2}{\frac{1}{2}\rho q_{nozzle}^2} \qquad (2)$$

Where a is the hole area. For the inlet manifold, c_{area} decreases with increasing $\frac{Q_\perp}{q_{nozzle}}$ (Fig. 1 and 2), which tends to increase q_{nozzle} along the manifold even with constant diameters like in Fig 7. For the outlet manifold, the opposite happens because the flux perpendicular to the nozzle, $Q_\perp$, creates a local pressure drop that increases q_{nozzle} with increasing $\frac{Q_\perp}{q_{nozzle}}$.

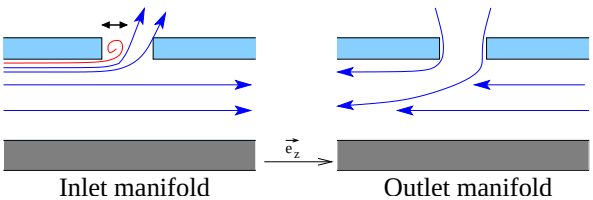

Figure 2: In the inlet manifold, the flow perpendicular to the nozzle ($Q_\perp$) reduces the effective area of the hole. The opposite happens in the outlet manifold.

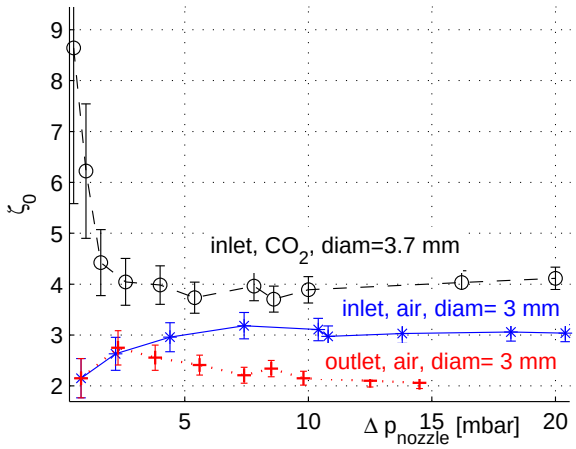

Figure 3: Nozzle flow resistance coefficient for constant diameter and $Q_\perp = 0$ obtained from eq. (2). The values for $\Delta p < 4\,mbar$ are wrong because the flux measurements were no longer accurate for low pressures; this is particularly clear for CO_2 because a proportional law was used to translate the values from an air calibrated flow-meter. This law fails for flows in the lower part of the flow-meter range. As long as Δp_{nozzle}¿4 is always true along the manifolds, this shows that ζ_0 can be assumed independent of the pressure.

Direct measurements of c_{area} were difficult; ζ measurements were therefore preferred for nozzles

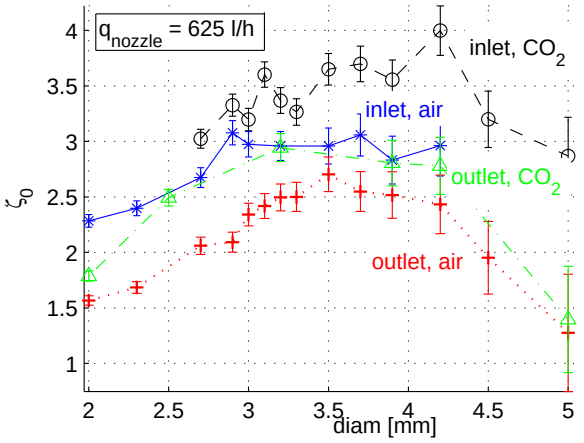

Figure 4: Nozzle resistance coefficient for $q_{nozzle} = 625\,l/h$ and $Q_\perp = 0$. The pressure is not constant but ζ_0 is independent on the pressure (see Fig. 3).

of constant diameters along the manifold (Fig. 5) and for nozzles of varying diameters in a differ-

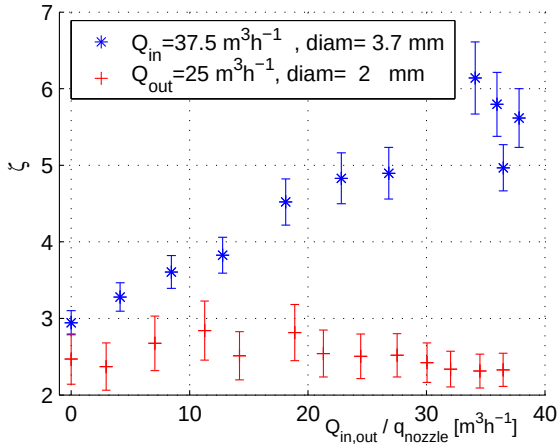

Figure 5: Nozzle resistance coefficients for constant diameters.

ent setup were the flux perpendicular to the nozzle $Q_\perp$ was zero, which allows to set $c_{area} = 1$ and measure ζ_0 from eq. (2). Figure 3 shows that ζ_0 can be assumed independent of Δp_{nozzle}. In addition, for $Q_\perp = 0$ and constant diameters, eq. (2) gives $\Delta p(q_{nozzle})$; ζ_0 is therefore also independent on q_{nozzle}. From the experiment, ζ_0 depends therefore only on the diameters (Fig. 4) and can even be assumed constant for diameters between 3 and 4.2 mm.

The dependence of ζ on $Q_\perp/q_{nozzle}$ was not significantly different for lower pressures (i.e. for smaller Q_{in} or bigger holes); eq. (2) is therefore valid and ζ can be found from the measurement of ζ_0 for different diameters and one measurement of $\zeta(Q_\perp/q_{nozzle})$

The thickness of the skin of the membrane in which the holes are drilled might influence the geometry of the flow. The thickness used for the mock-up was 1.5 mm instead of 1.3 mm for the final set-up and measurements with 2 mm thick holes gave the same ζ_0 as 1.5 mm thick holes.

3.2 Flow along the manifold

The pressure loss along the manifold was described by the D'Arcy friction factor [6]:

$$f = \frac{\Delta p_{friction}}{\frac{\Delta z}{D_H}\frac{1}{2}\rho v^2} \tag{3}$$

Where D_H is the hydraulic diameter and Δz the length along which the pressure is measured. f is strongly dependent on Re and it's value is interpolated in the program according to the *Moody chart* found in [6]. This friction factor acts in the opposite way than the effective area coefficient in the sense that it makes q_{nozzle} decrease along the manifold.

3.2.1 Effect of bending

According to formulas given in [5], the pressure loss for a 2 meters circularly bent pipe of rectangular cross section was substracted to the pressure loss calculated for a straight pipe of same section. The result is an additional pressure drop of 1.6 mbar in the bent case for a $50\,m^{-3}h^{-1}$ flow. The pressure drop along the manifold being smaller than along an open pipe due to the constant decrease of $Q_\perp$; the difference should be lower and therefore negligible.

Another effect of bending that might affect the flow distribution is the pressure difference perpendicular to the flow. This results in an increase of the velocity on the inside of the bend, where the holes are located in the case of the inlet manifold. The consequence should be a more important decrease of the effective area of the holes on the entrance of the manifold and therefore a more important increase of q_{nozzle} at the end that should compensate

losses due to the bending. This effect should however be negligible.

3.3 Regime

The flow is changing regime within the system at a position along z that depends on the total flow (Fig. 6).

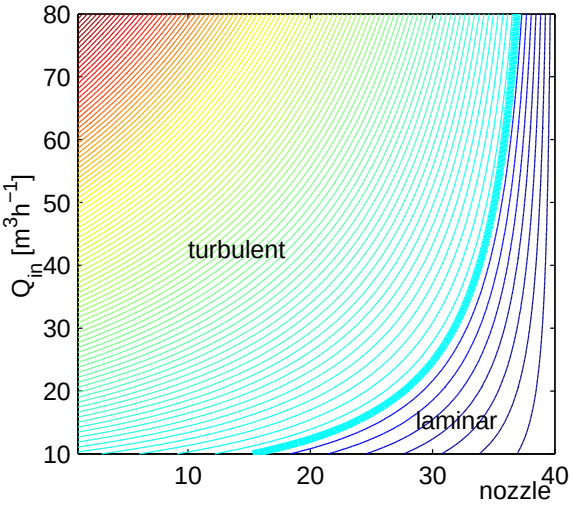

Figure 6: Reynolds number contours for the CO_2 flow in the inlet manifold.

4 Results

4.1 Model validation

For the inlet manifold, three different kinds of evolutions of q_{nozzle} along $\overrightarrow{e}_z$ have been observed; monotonously decreasing when $\frac{\partial p_{friction}}{\partial z}$ dominates, with a minimum when $\frac{\partial p_{friction}}{\partial z}$ is comparable to $\frac{\partial p_{nozzle}}{\partial z}$ due to the decrease of $Q_\perp/q_{nozzle}$ and monotonously increasing when the latest dominates (Fig. 7). These three features were well reproduced by the program.

For the outlet manifold, q_{nozzle} is always monotonously decreasing for constant diameters. Fig. 8 shows a good match between the model and the measured results for air.

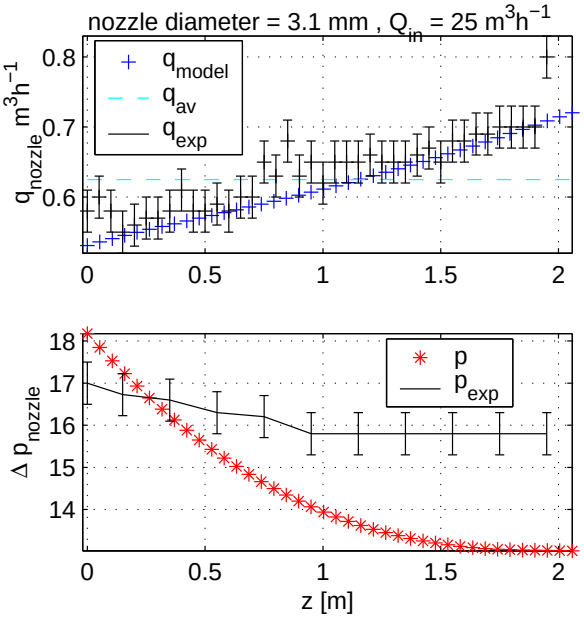

Figure 7: Profiles along the inlet manifold for air and $Q_{in} = 25$ m^3 h^{-1}. The model fits well with q_{nozzle} measurements. $\zeta(\frac{Q_\perp}{q_{nozzle}})$ used in the model was measured for $Q_{in} = 37.5$ m^3 h^{-1} and holes of 3.7 mm diameters, showing that the fit is good even for different conditions. The hump on $q_{nozzle}(z)$ at $z = 0.95$ m is due to imperfections at $z = 1$ m where two aluminium profiles are appended.

4.2 Optimized diameters for CO_2

The cross sections of the final inlet and outlet manifolds were respectively set to 42 x 6.3 mm and 42 x 7.3 mm.

A first step in the optimisation for a given Q_{in} consists in finding the constant diameter so that $q_{nozzle}(z)$ has a minimum in the center of the inlet manifold (Fig. 9). The value found is 4 mm for CO_2. In a second approach, the diameters can be changed to a flat q_{nozzle} profile.

The outlet manifold $q_{nozzle}(z)$ does not exhibit a minimum. As long as the results for constant diameters have $\Delta q_{nozzle} = 70\,\%$ for $Q_{in} = 25$ m^3 h^{-1}, a variation of the holes diameters is necessary (Fig. 10).

Increasing Q_{in} and Q_{out} results in a counter-clockwise rotation of the q_{nozzle} profile. However, this rotation is small enough to allow the use of the optimal holes diameters found for 25 m^3 h^{-1} for 12.5 m^3 h^{-1} and 37.5 m^3 h^{-1}.

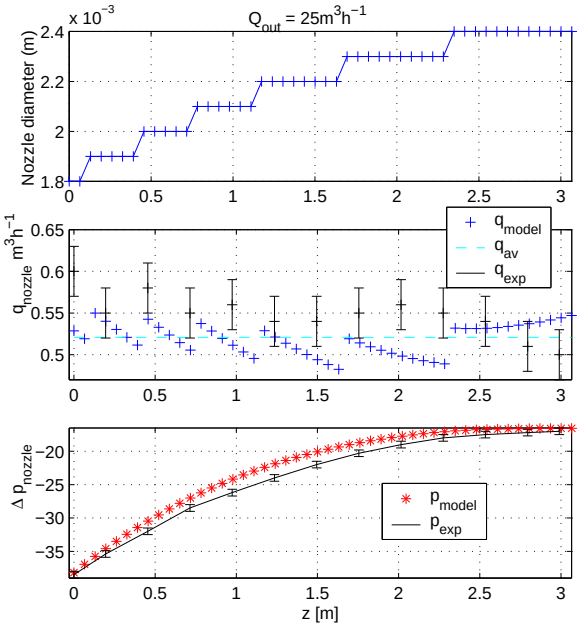

Figure 8: Profiles along the outlet manifold for air and $Q_{in} = 25\ \mathrm{m^3\,h^{-1}}$.

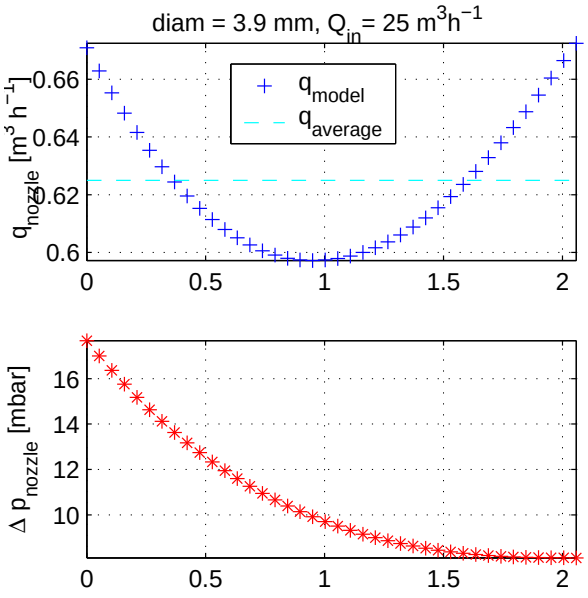

Figure 9: Profiles along the inlet manifold for CO_2 and $Q_{in} = 25\ \mathrm{m^3\,h^{-1}}$. Holes diameters were set 3.9 mm because of numerical instabilities for 4 mm that made the program not convergent.

4.3 Inlet and Outlet wyes

An ANSYS simulation was run using FLOTRAN to calculate the pressure drop at the wyes linking the two half manifolds (Fig. 11). Assuming a stationary irrotational flow, for the inlet manifold, the pressure increases due to the diverging flow. This was still true in the turbulent case, where local energy losses don't cancel completely this pressure increase. This was checked using the turbulent solver (Table 1).

	Inlet			**Outlet**		
Q_{tot} [m^3h^{-1}]	25	50	75	25	50	75
section [mm]	**42 x 6.3**			**42 x 7.3**		
Δq_{nozzle} [%]	16	12	16	23	24	25
Δp_{manif} [mbar]	5	18	34	16	50	120
Δp_{wye} [mbar]	-1	-6	-13	12	42	94

Table 1: Important results for final inlet and outlet manifolds.

4.4 Turbulence influence on the straws

Tests with a 45° quadrant consisting in 4 straw layers with radiators and membrane showed no visible vibration. In addition, the flux from the holes impinges on the hard glued tip of the straws, which is the less sensitive part. The same test was made more thoroughly in a test-beam, showing low perturbation on the position measurement [4].

5 Discussion

The D'Arcy friction factor had to be rescaled by a factor 3 to match the measured pressure values for the outlet manifold (Fig. 8). For the inlet manifold, a scaling factor could not be used for the program did not converge, but it would be necessary to use a scaling factor of about 0.2 to match the pressure measurements of Fig. 7. This shows the limits of the model.

The chosen q_{nozzle} profiles for half manifolds give two maxima and two minima along the wheels perimeter. In addition, the flux can be assumed more homogeneous in the detector volume than at

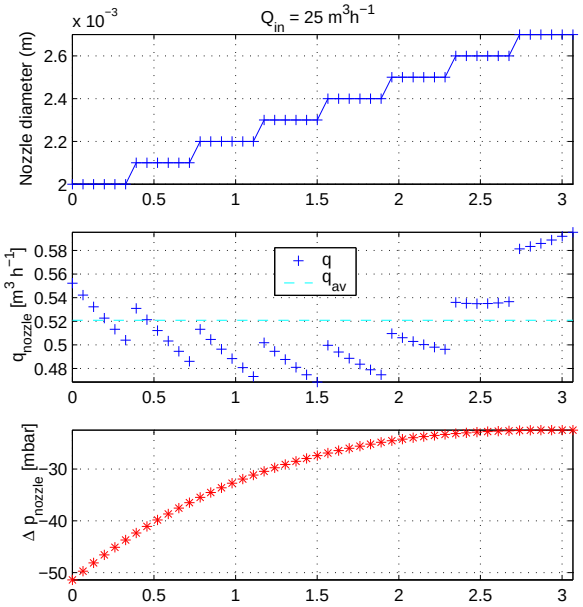

Figure 10: Profiles along the outlet manifold for CO_2 and $Q_{in} = 25\ \mathrm{m^3\,h^{-1}}$.

the nozzles of the manifolds due to the smoothing out of the flux inhomogeneities by the resulting pressure gradients in the communicating detector volume. This means that the flow variation will be lower than 25% for all group of wheels in the detector.

The results for group of wheels of C-type with $Q_{tot} = 75\ \mathrm{m^3\,h^{-1}}$ might be subject to changes as long as the design of these wheels is not yet final.

The cross section of the outlet manifold was set to the maximal values allowed by the structural and mechanical requirements on the membrane in which the manifolds are embedded. The only other way to try and decrease the manifold pressure drop (Δp_{manif}) without a deterioration of the flux distribution is change the geometry of the flow through the holes or the number of holes; an attempt in using 90° elbows instead of simple holes with their openings oriented towards the incoming flux to take advantage of the kinetic pressure of the flow to have an increasing $\zeta(\frac{Q_\perp}{q_{nozzle}})$ (like for the inlet manifold) gave similar pressure drops due to the increased losses in the elbow itself. This shows that, for the largest apertures that optimize the flow distribution, the pressure loss is determined by the friction losses along the manifold, which are larger for the outlet manifold than for the inlet manifold because it is longer.

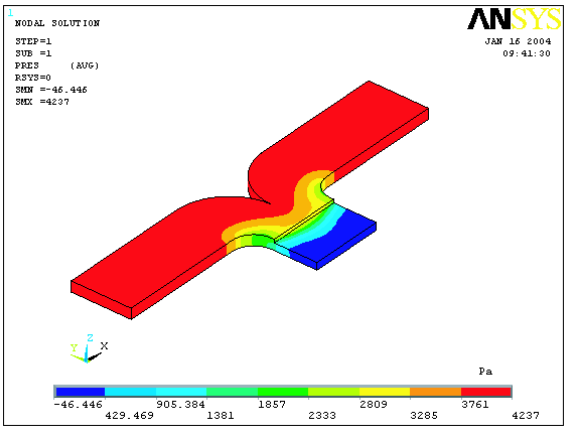

Figure 11: Static pressure contours for CO_2 in the outlet wye for a flux of 50 $\mathrm{m^3\,h^{-1}}$. The radius of the bends are 29 mm, the cross section of the manifolds 42x7.3 mm.

The model was used to see the dependance of Δp_{manif} on the number of holes. The result is a minimum for 55 holes with a difference of 1 mbar for $Q_{out} = 25\ \mathrm{m^3\,h^{-1}}$ relative to the result for 48 holes, which is negligible.

6 Conclusion

The hydraulic diameters of the manifolds were set to their maximum values in the confined space of the Inner Detector.

The dependence of the nozzle flow resistance coefficient on the perpendicular flux in the manifold allowed to optimize the inlet manifold with constant diameter holes, what simplified the production line and allowed a flux variation smaller than 16% at the inlet of the detector.

For the outlet manifold, a diameter distribution was proposed in order to have a flux variation smaller than 24 %. The overall pressure drop of 92 mbar for A-type group of wheels cannot be reduced further with the given structural requirements on the wheel membrane.

References

[1] The ATLAS collaboration, *ATLAS Inner detector Technical Design Report*, Vol. II, ATLAS TDR 5, CERN/LHCC 97-17, 1997

[2] J. Godlewski et al., *Inner Detector Thermal Management and Environmental Gas*, technical note ATL-IC-EN-0009, CERN, 2003

[3] P. Skarby, *The Straw Cooling System in the ATLAS TRT*,Technical note ATC-TL-EN-0002, CERN, 2002

[4] M. Anderson et al., *Studies of wire vibrations in TRT straw tubes*, Technical note ATL-INDET-2000-018, CERN, 2000

[5] I.E. Idelchik, *Handbook of Hydraulic Resistance*, 3^{rd} ed., CRC Press, 1994

[6] Hoffman, *Gas Dynamics*, vol. 1, John Wiley & Sons, New York, pp 256-257, 1976

A Poiseuille flow in rectangular pipes

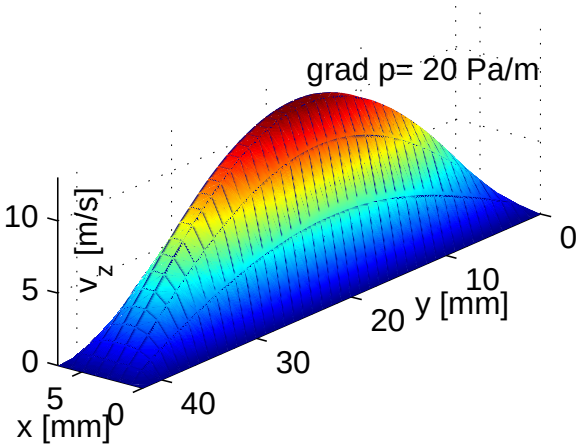

Figure 12: Velocity profile in the manifold cross-section for a fixed pressure drop.

The Navier-Stokes equations with zero velocity boundary conditions for an incompressible permanent flow give a system that can be solved as an eigenvalue problem using a Fourier expansion. The result for the velocity is;

$$u(x,y) = \sum_{m=1}^{\infty}\sum_{n=1}^{\infty} \frac{-C_{m,n}}{\eta}\frac{\partial p}{\partial z}\sin(\frac{m\pi y}{w})\sin(\frac{n\pi x}{h})$$

$$C_{m,n} = \frac{16}{mn\pi^2\left[\left(\frac{m\pi}{w}^2\right)+\left(\frac{n\pi}{h}^2\right)\right]}$$

w and h are respectively the width and height of the pipe.